Bulletin of Engineering Geology and the Environment (2021) 80:519–531
https://doi.org/10.1007/s10064-020-01932-6

ORIGINAL PAPER

A new quantitative method to identify the crack damage stress of rock using AE detection parameters

Chen Wu[1] · Fengqiang Gong[1,2] · Yong Luo[1]

Received: 13 January 2020 / Accepted: 16 July 2020 / Published online: 29 July 2020

Abstract

The quantitative determination of crack damage stress is of significant importance for investigating rock deformation and failure. In this study, a new quantitative method for determining the crack damage stress of rock materials was proposed based on acoustic emission (AE) signal detection. Ten rock materials were subjected to uniaxial compression testing, during which real-time AE signals and axial, lateral, and volumetric strain values were recorded. The AE cumulative count curves of the different rock materials were calculated based on the AE counts. These curves were divided into three stages as the axial stress increased: the slowly increasing stage, the steady stage, and the sharply increasing stage. The point where the sharply increasing stage began was defined as the P_R point and could be accurately determined based on a fitting optimization method. Then, the damage stress was calculated by using the crack volumetric strain model. Finally, the relationship between the R stress (axial stress corresponding to the P_R point) and the crack damage stress was investigated for the ten rock materials. The results showed that there was a good correspondence between the R stress and the crack damage stress. Hence, the R stress can be used to determine the crack damage stress and the starting point of the unstable crack growth stage in rock materials.

Keywords Rock mechanics · Crack evaluation · Quantitative method · Acoustic emission · Damage stress

Introduction

The failure process of rock materials is controlled by the development and evolution of internal microcracks (Martin 1993; Zhou and Wang 2016; Pepe et al. 2018; Peng et al. 2018; Wang and Li 2015). The yielding evolution process of rock materials is a macroscopic manifestation of crack initiation and propagation processes (Diederichs et al. 2004; Zhu et al. 2007; Chen et al. 2019). Additionally, the deformation process of rock materials under compressive loading is nonlinear. The process of rock deformation can be roughly divided into four stages based on crack evolution characteristics: the crack closure stage, the no crack initiation stage, the crack initiation and stable propagation stage, and the unstable crack propagation stage. Furthermore, there are several important rock stress thresholds in this process: the crack compaction stress (σ_{cc}), crack initiation stress (σ_{ci}), crack damage stress (σ_{cd}), and peak stress (σ_f), which are characterized as the stress levels corresponding to the end points of the four deformation stages (Diederichs et al. 2004; Zhou et al. 2004 and 2008; Zhou 2005; Martin 1997; Martin and Chandler 1994).

The determination of the above stress thresholds is of great significance for understanding mechanical mechanisms and performing failure predictions for rocks under compression. Extensive laboratory and field investigations have been performed to analyze these thresholds (Martin 1997; Nicksiar and Martin 2013). Martin (1993, 1997) proposed determining σ_{cc}, σ_{ci}, and σ_{cd} by using a crack volumetric strain model. They hypothesized that σ_{ci} can be used to predict the failure of the rock surrounding tunnels. Liu et al. (2009) used a linear regression technique to determine σ_{ci} and σ_{cd} based on the volumetric strain curve of granite under various confining pressures. Nicksiar and Martin (2012) summarized five strain-based methods in laboratory compression tests of σ_{ci} and σ_{cd} and proposed a lateral strain method for low-porosity rocks. Gong and Wu (2019) evaluated the relationships between the crack stress thresholds and the load-unload response ratio curves of ten rock materials. Moreover,

✉ Fengqiang Gong
fengqiangg@126.com

[1] School of Resources and Safety Engineering, Central South University, Changsha 410083, Hunan, China

[2] School of Civil Engineering, Southeast University, Nanjing 210089, China

they proposed a method for determining σ_{cc} and σ_{cd} based on the load-unload response ratio theory.

Furthermore, the rock damage and failure process is also associated with acoustic emission (AE) signals. AE detection can capture the AE signals that are generated by the formation of local damage inside rocks, allowing researchers to monitor the rock damage and deformation process (Koerner et al. 1981; Cai et al. 2007a, b; Moradian et al. 2010). Therefore, many researchers have used AE parameters during compression testing to determine the stress thresholds of rock materials (Mlakar et al. 1993; Eberhardt et al. 1997; Eberhardt et al. 1998; Zhang and Wong 2013). Zhou et al. (2014) found that the AE count rate can qualitatively reflect the crack evolution characteristics in different deformation processes and can be used to qualitatively evaluate σ_{ci} and σ_{cd}. Eberhardt et al. (1998) suggested that σ_{ci} values during laboratory uniaxial compression tests of rock materials could be determined using the AE count method. Furthermore, AE detection parameters can be used to classify crack stress thresholds (Zhou et al. 2019; Zhang et al. 2019). Therefore, more in-depth research is necessary to investigate crack stress thresholds based on AE monitoring parameters (Eberhardt et al. 1998; Huang and Li 2017; Yang et al. 2017).

In the present study, uniaxial compression tests were performed to investigate the engineering properties of ten rock materials. The objectives of these experiments were to determine the crack stress thresholds and understand the damage process in rock materials using AE cumulative count curves. To this end, real-time AE events in the rock materials were captured during uniaxial compression tests. In addition, the relationships between the inflection points in the AE cumulative count curves and the stress thresholds were analyzed and discussed. This work offers a quantitative determination of crack stress thresholds during the rock deformation process.

Crack development in rock materials subjected to uniaxial compression

It is known that the rock material damage process is accompanied by several deformation stages: the compaction stage, the elastic deformation stage, the crack initiation and expansion stage, and the unstable crack propagation stage (Martin 1993, 1997). The crack initiation and expansion stage and unstable crack propagation stage of rock are close to rock failure. Furthermore, the determination of the stress thresholds associated with these deformation stages is significant for rock instability predictions (Cai et al. 2004). Extensive theoretical and experimental studies on the determination of crack stress thresholds have been performed, and various determination methods have been proposed. In the determination of crack stress thresholds, studies have typically been based on fracture mechanics methods (Wei et al. 2017a, b; Du et al. 2020; Liu et al. 2018). Moreover, it is generally understood that the crack volumetric strain model (Martin and Chandler 1994) is the most widely used method for identifying the stress thresholds of rock materials (Eberhardt et al. 1998; Cai et al. 2004; Wang et al. 2012; Wen et al. 2018; Kong et al. 2018).

The main equation for the crack volumetric strain model for uniaxial compression conditions can be written as follows (Martin and Chandler 1994; Eberhardt et al. 1998; Cai et al. 2004; Cai 2010; Wang et al. 2012):

$$\varepsilon_{\mathrm{V}}^{e} = \varepsilon_{\mathrm{V}} - \frac{1-2\nu}{E}\sigma_1 \tag{1}$$

where $\varepsilon_{\mathrm{V}}^{e}$ is the calculated crack volumetric strain, ε_{V} is the volumetric strain, σ_1 is the uniaxial stress, and E and ν are the elastic modulus and Poisson's ratio of the rock material, respectively.

On the basis of Eq. (1), the crack initiation and propagation process of a rock material could be investigated with the calculated crack volumetric strain. Specifically, Fig. 1 shows the axial strain, volumetric strain, and calculated crack volumetric strain of a rock material (taking Yueyang granite as an example) subjected to uniaxial compression conditions. Moreover, the different deformation stages and stress thresholds of Yueyang granite can be accurately distinguished and systematically analyzed as follows.

(1) The crack closure stage (I) ends at a stress level of approximately 0.14 times the peak stress of the rock material. Additionally, σ_{cc} can be determined from the stress level corresponding to the starting point of the horizontal section based on the calculated crack volumetric strain curve.
(2) The axial stress range of the no crack initiation stage (II) is 0.14–0.30σ_f. The stress-strain curves in this stage maintain a linear relationship. The AE count in this stage is much lower than that in the compaction stage.
(3) The initial stress level of the crack initiation and stable propagation stage (III) is defined as σ_{ci}. In this stage, the AE count begins to increase as the stress increases, which indicates that new microcracks are generated and begin to propagate.
(4) The stress level corresponding to the starting point of the unstable crack propagation stage (IV) is identified as σ_{cd}. Additionally, σ_{cd} is typically defined as the axial stress corresponding to the inflection point of the volumetric strain curve, where the AE count increases sharply (Cai et al. 2004; Wang et al. 2012; Wen et al. 2018; Kong et al. 2018; Cai et al. 2007a, b; Cai 2010).

Test methodologies

Specimen preparation

To investigate the AE characteristics and stress thresholds of different rock materials through uniaxial compression testing,

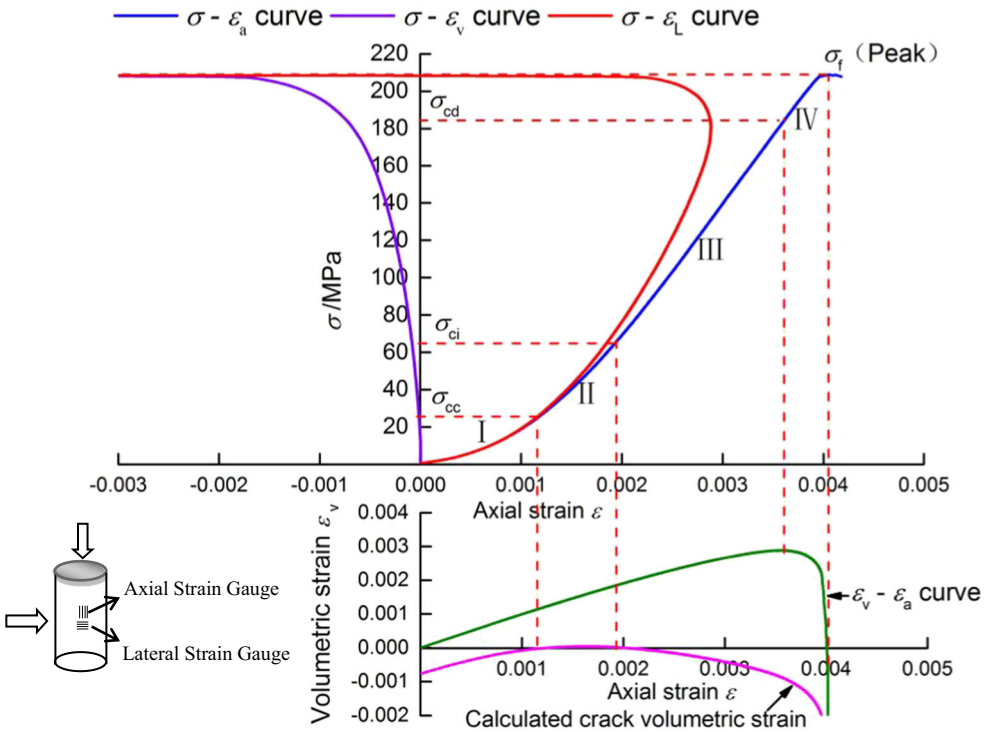

Fig. 1 Stress-strain diagram showing the different stages of crack development stages (the crack compaction stage, elastic deformation stage, crack initiation and expansion stage, crack unstable growth stage) (Based on Martin 1997) (σ: axial stress, ε_a: axial strain, ε_v: volumetric strain, ε_L: lateral strain)

ten rock specimens were selected for this study (Yueyang granite, fine granite, Qingshan granite, red granite, red sandstone, green sandstone, yellow sandstone, Henan limestone, slate, and Leiyang white marble). The ten rock specimens are presented in Fig. 2. All specimens were processed into standard cylinder shapes with dimensions of Φ50 mm × 100 mm, as recommended by the American Society for Testing and Materials. The upper and lower ends of the rock specimens were ground to ensure that they were parallel and smooth.

Test equipment

Uniaxial compression testing was performed on an MTS815 electrohydraulic servo testing machine (MTS, USA), which is shown in Fig. 3. This testing machine is a multifunctional electrohydraulic servo tester that was specially designed for rock testing. Uniaxial compression, triaxial compression, and pore water pressure testing of rock materials can be carried out with this machine. The test system has a maximum load capacity of 4600 kN and can supply a maximum confining stress of 140 MPa.

Test procedure

In the uniaxial compression test, axial compression was applied to the rock specimens with a loading rate of 12 kN/min until the specimens failed. AE transducers (PAC, USA) were used to record AE data during the testing process. The trigger threshold of AE was set to 45 dB for each test, and full waveform data were recorded with a sampling rate of 1 MHz. Two AE transducers were used during the uniaxial compression test. The AE transducer array was symmetrical, and the AE probes were contact with the rock specimens to provide good acoustic coupling between the rock specimens and the sensors.

Testing results

Rock failure modes

In order to analyze the failure modes of different rock materials in uniaxial compression tests, Fig. 4 presents images of the typical failure modes of the ten different rock materials, and Table 1 explicitly summarizes these failure modes.

Conjugate shear failure was the main failure mode of the Yueyang granite and fine granite specimens under uniaxial compression conditions. Additionally, double cones were formed in these rock specimens. Tensile cracks appeared on the surfaces of these rock specimens, and the specimens failed rapidly after reaching the peak stress. This failure was accompanied by ejection phenomena. The main failure mode of the green sandstone and yellow sandstone was internal conjugate shear. A double shear plane was formed in these rock specimens, which was accompanied by fragment ejection when the specimens failed. The main failure mode of the Henan limestone, slate, and Leiyang white marble was open-shear

Fig. 2 Ten rock specimens

composite failure. Moreover, double cones were also formed in these rock specimens.

AE cumulative count curves in the laboratory compression tests

Representative AE cumulative count curves for the ten rock materials were obtained during the uniaxial compression tests, as shown in Fig. 5. The AE cumulative count curves show clear regularity. With increasing axial strain, the AE cumulative count curves of the rock materials initially increase gently and then remain relatively stable for a time. Finally, the AE cumulative count curves increase sharply as the rock specimens approach failure (Wei et al. 2016). Furthermore, it can be observed that the AE cumulative count curves of the rock materials have two inflection points. The evolution states of the cracks in each rock specimen change after these inflection points, indicating that there is a correlation between the axial stresses corresponding to the inflection points and the stress thresholds of the rock specimens.

Lateral strain and volumetric strain in the laboratory compression tests

Figure 6 illustrates the axial stress-lateral strain curves, axial stress-volumetric strain curves, and volumetric strain-axial strain

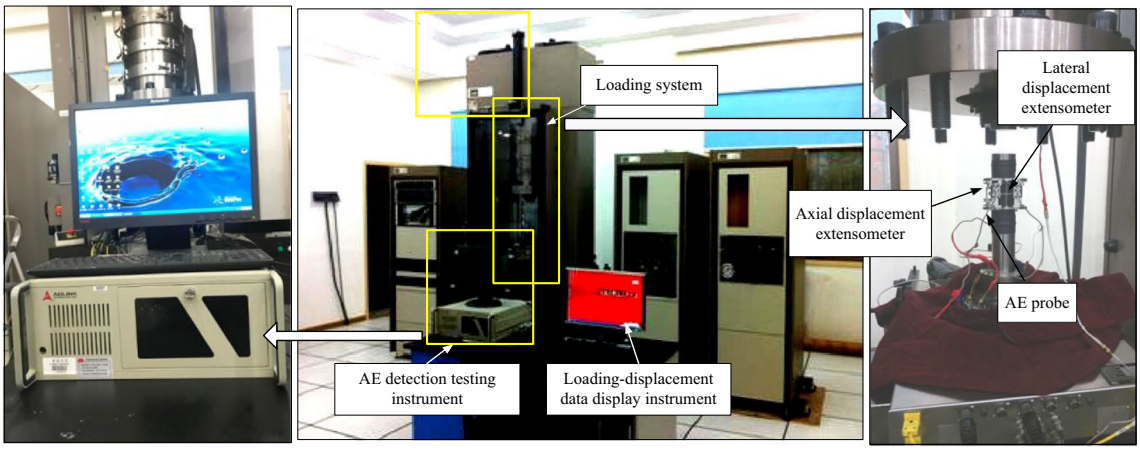

Fig. 3 MTS815 electrohydraulic servo testing machine

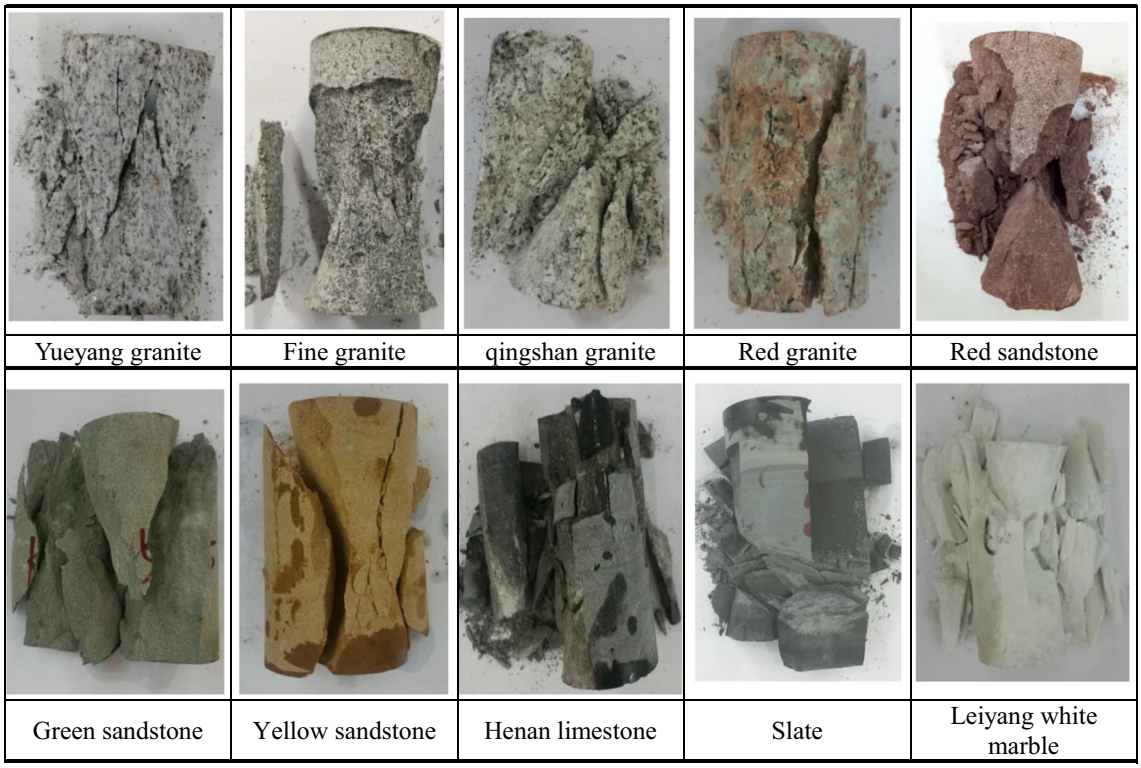

Fig. 4 Failure modes of ten rocks under the uniaxial compression test

curves of nine rock materials (the curves of Yueyang granite shown in Fig. 1). There is inflection point in the axial stress-volumetric strain curves of the ten rock materials, and σ_{cd} could be determined according to the crack volumetric strain model (Martin and Chandler 1994; Eberhardt et al. 1998; Cai et al. 2004; Wang et al. 2012). Specifically, σ_{cd} could be identified based on the inflection points of the axial stress-volumetric strain curves. In addition, after this inflection point, the curves of the rock specimens begin to decrease, and the rock cracks enter the unstable crack development stage (Cai et al. 2004; Cai 2010).

Fitting optimization method

As shown in Fig. 7, the AE cumulative count curves can be roughly divided into the slowly increasing stage (I), the steady stage (II), and the sharply increasing stage (III) as the axial stress increases (Yueyang granite is shown as an example). With increasing axial stress, the AE count decreases because the microcracks in the rock are gradually compressed. However, the AE count is relatively stable in the steady stage of the AE cumulative count curve. In the sharply increasing stage, which follows the steady stage, AE count exhibits a sharply increasing trend with increasing axial stress, indicating that the internal cracks in the rock material have entered the unstable growth stage. Note that there is an inflection point between the steady stage and the sharply increasing stage of the AE cumulative count curves. To better capture and distinguish this inflection point, it is defined as P_R point.

Table 1 Failure mode of the different rock materials during uniaxial compression testing

Rock type	Yueyang granite	Fine granite	Qingshan granite	Red granite	Red sandstone
Main failure mode	Open-shear composite failure, double cones formed inside rocks	Open-shear composite failure, double cones formed inside rocks	Double-sided shear failure	Internal conjugate shear failure	Open-shear composite failure
Rock type	Green sandstone	Yellow sandstone	Henan limestone	Slate	Leiyang white marble
Main failure mode	Internal conjugate shear, double shear plane formed in rocks	Internal conjugate shear failure	Open-shear composite failure, double cones formed inside rocks	Double-sided shear failure	Open-shear composite failure, double cones formed inside rocks

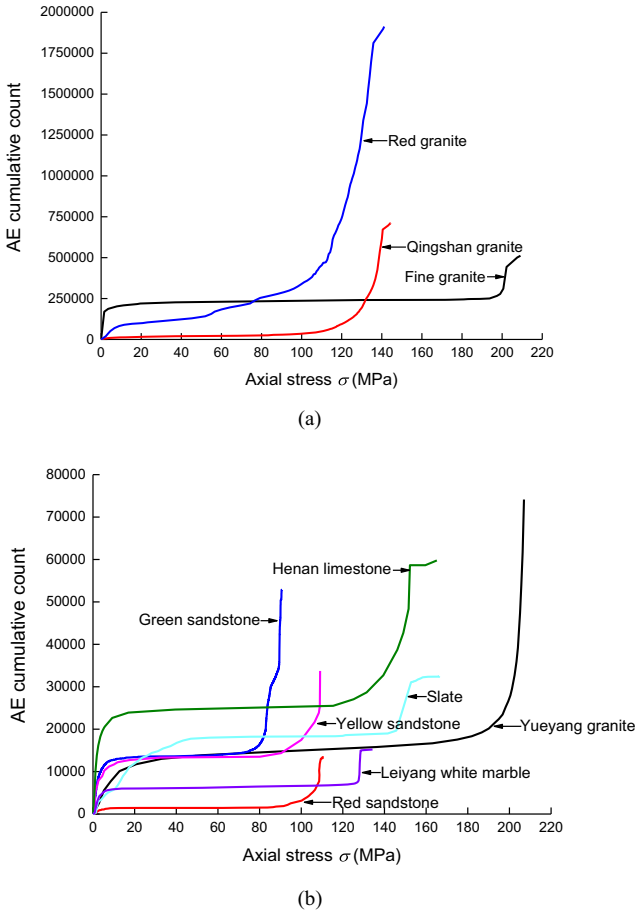

Fig. 5 Representative AE cumulative count curves of ten rocks under the uniaxial compression test

To quantitatively determine the P_R point of a rock material, we propose a fitting optimization method consisting of the following steps:

Step 1: To accurately identify the inflection points of AE cumulative count curves, the data points comprising the AE cumulative count curve are divided into two parts (part I and part II) according to the axial stress (see Fig. 8).

Step 2: Part II is fitted by a fourth-degree polynomial, and the fitting function for this part is obtained. If the fitting coefficient of the fitting function is less than 0.996, then the maximum deviation between the fitting line and the AE cumulative count data points is investigated (i.e., the residual between the fitting value and the actual data points in the AE cumulative count curve is calculated).

Step 3: The data points in the AE cumulative count curve are reduced in increments of 1% from one end of the maximum deviation between the fitting line and the AE cumulative count data points. The remaining data points are fitted again by a fourth-degree polynomial. This step is repeated until the fitting coefficient of the fitting function is greater than 0.996.

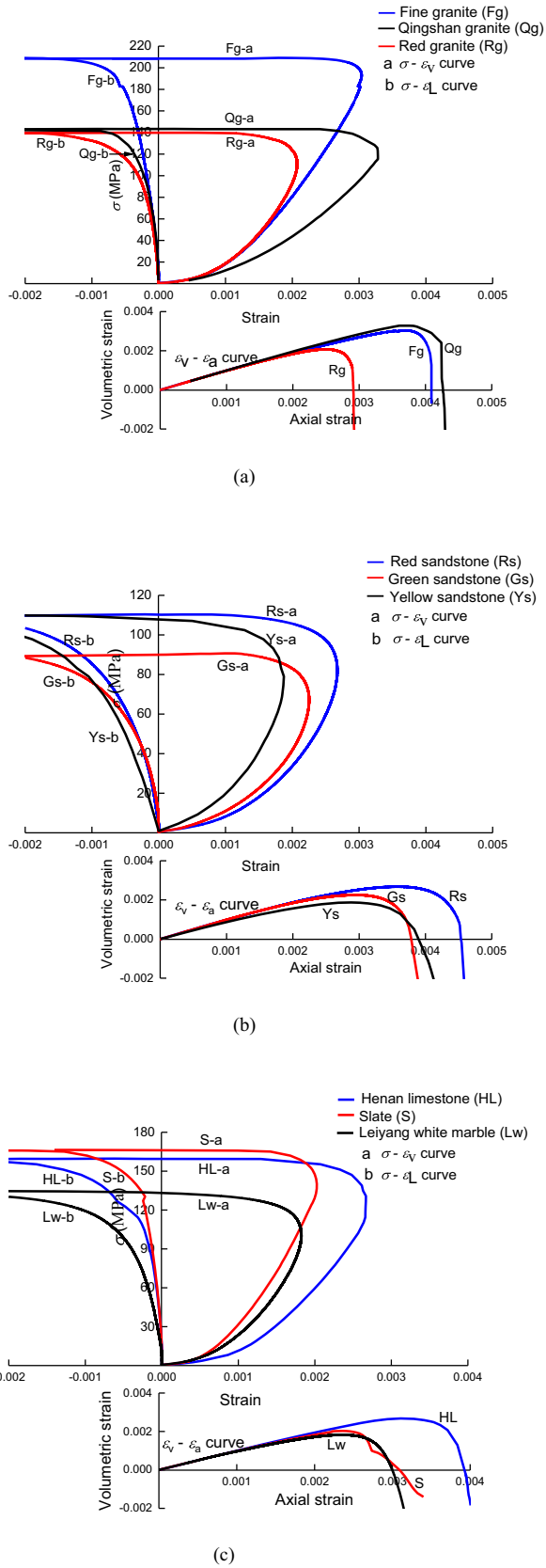

Fig. 6 Axial stress-lateral strain curves, axial stress-volumetric strain curves, and volume strain-axial strain curves of nine rocks during the uniaxial compression test

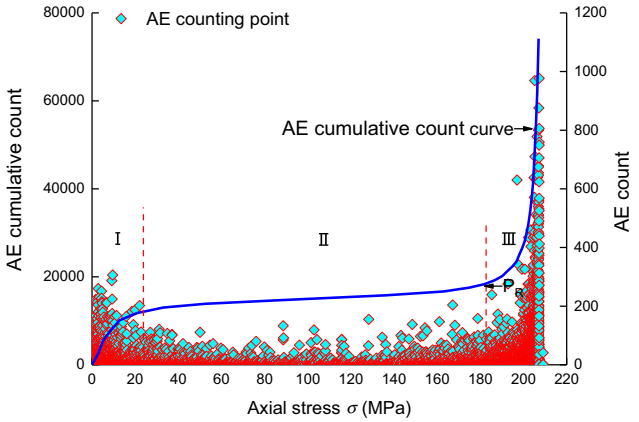

Fig. 7 Three different stages of AE cumulative count curve

Step 4: The first and second derivatives of the fitting formula are calculated. It is known that the second derivative characterizes the concavity and convexity of the fitting curves (Liu et al. 2013).

Step 5: Data point corresponding to the maximum value of the second derivative could be recognized as P_R point.

Note that steps of the fitting optimization method could be programmed to determine the P_R point more accurately based on a scientific method. Taking the AE cumulative count curve of Yueyang granite as an example, the AE cumulative count curve can be brought into the operation program (illustrated in the Appendix) by using a MATLAB script. When the fitting coefficient is greater than 0.996, the coordinates of the P_R point are (183.32, 18486), as shown in Fig. 9.

Relationship between the R stress and the damage stress

In this study, the axial stress corresponding to the P_R point was characterized as the R stress (σ_R^{AE}). Based on the AE cumulative count curves for the ten rock materials, σ_R^{AE} was generated with the fitting optimization method. Moreover, based on the crack volumetric strain model, σ_{cd} is the axial stress corresponding to the inflection point of the axial stress-volumetric strain curve (Martin and Chandler 1994; Martin 1997). Furthermore, it can be concluded that σ_{cd}^{AE} is largely consistent with the axial stress corresponding to the inflection point of the axial stress-volumetric strain curve (shown in Fig. 10).

Furthermore, to quantitatively investigate the relationship between σ_S^{AE} and σ_{cd}, the values of σ_R^{AE} and σ_{cd} were determined for each rock specimen. Two rock specimens for each rock material were used in the uniaxial compression tests, and the σ_R^{AE} and σ_{cd} values obtained for each rock specimen are listed in Table 2. Moreover, the relative errors between σ_R^{AE} and σ_{cd} of the different rock specimens were investigated, and the relative errors are also listed in Table 2.

Additionally, the fitting relationship between σ_R^{AE} and σ_{cd} is illustrated in Fig. 11. Figure 11 shows that the fitting equation for σ_R^{AE} and σ_{cd} of the ten rock materials is $\sigma_{cd} = 1.01\sigma_R - 1.37$, and the coefficient of determination is 0.964. The coefficient of determination and the slope of the σ_S^{AE}–σ_{cd} fitting line are close to 1, which suggests that there is a relatively strong linear relationship between σ_R^{AE} and σ_{cd} in the uniaxial compression test. Note that σ_R^{AE} is basically equal to σ_{cd} in the uniaxial compression test. Moreover, it can be concluded that σ_R^{AE} could be used to distinguish σ_{cd} and the starting point of the dilation stage of rock materials.

Discussion

Eberhardt et al. (1998, 1999) used several approaches to identify crack stress thresholds for rock materials, including the moving point regression method and the AE signal cumulative curve method. The AE signal cumulative curve

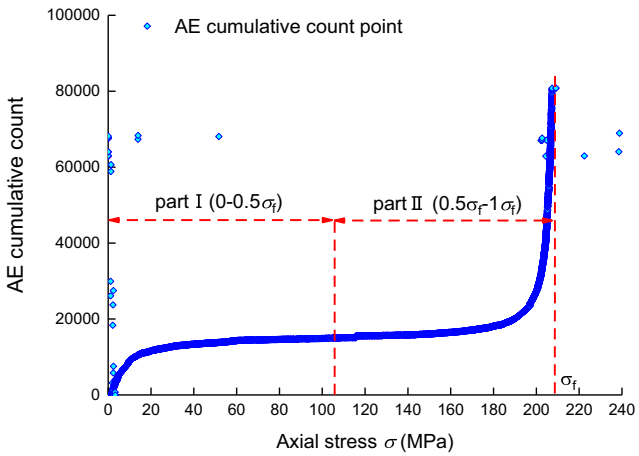

Fig. 8 Two parts of AE cumulative count curve in fitting optimization method

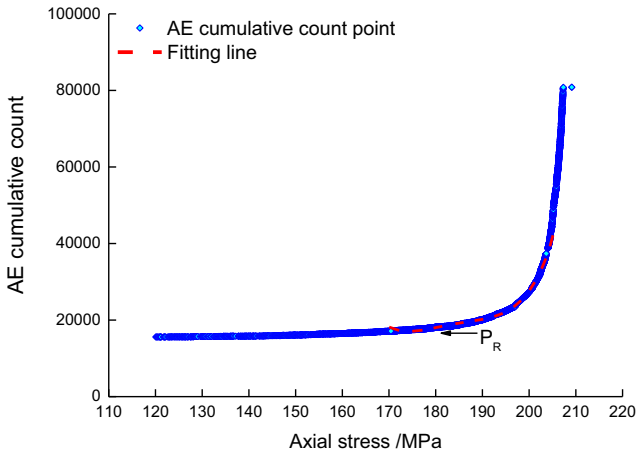

Fig. 9 Schematic illustration of P_R point determination from uniaxial compression tests using fitting optimization method

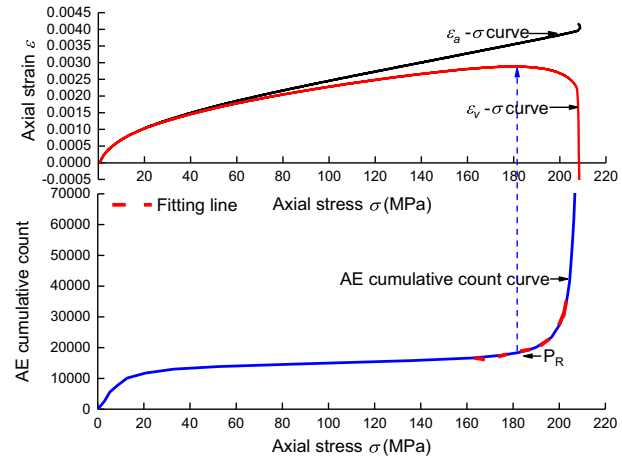

(a) Yueyang granite 1

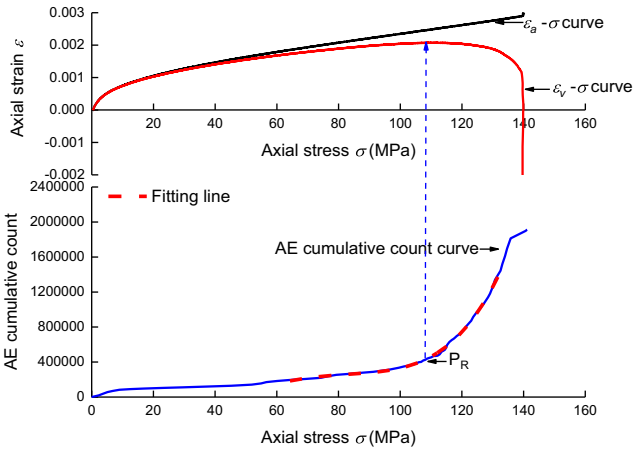

(d) Red granite 2

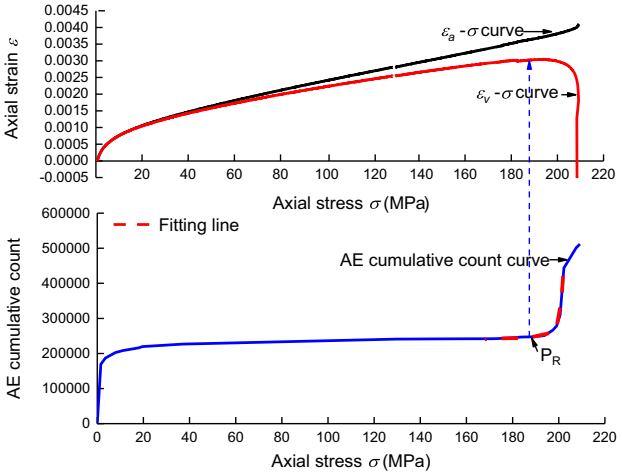

(b) Fine granite 1

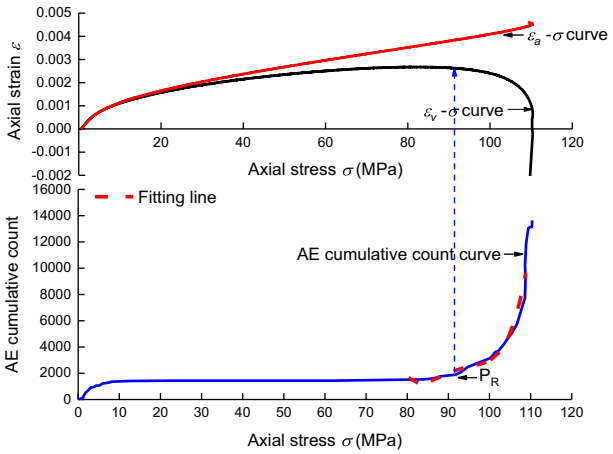

(e) Red sandstone 1

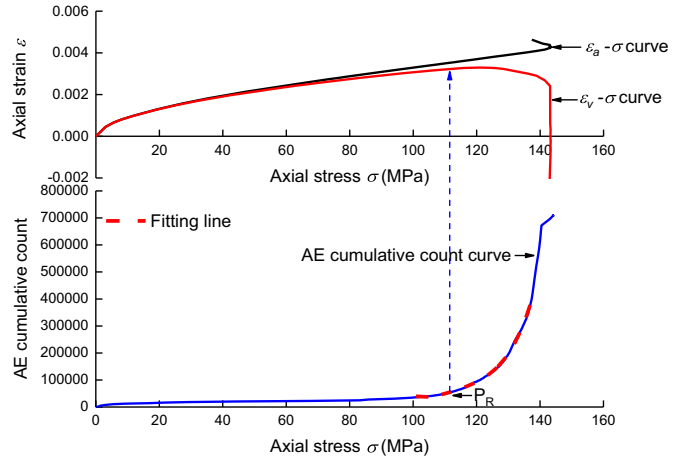

(c) Qingshan granite 2

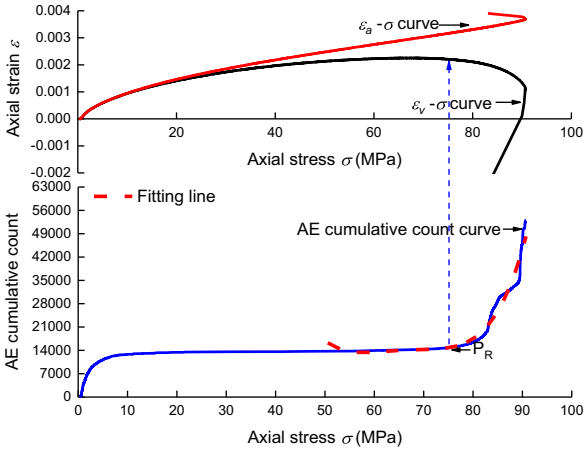

(f) Green sandstone 1

Fig. 10 Axial stress-strain curves, axial stress-volumetric strain curves, and AE cumulative count curves for ten rocks. **a** Yueyang granite 1. **b** Fine granite 1. **c** Qingshan granite 2. **d** Red granite 2. **e** Red sandstone 1. **f** Green sandstone 1. **g** Yellow sandstone 1. **h** Henan limestone 1. **i** Slate 2. **j** Leiyang white marble 1

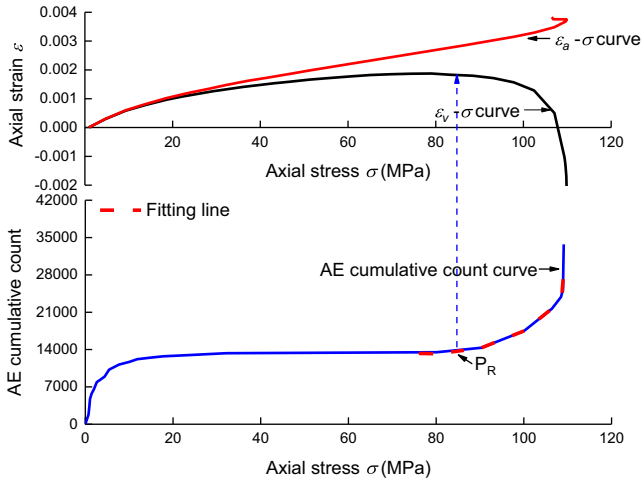

(g) Yellow sandstone 1

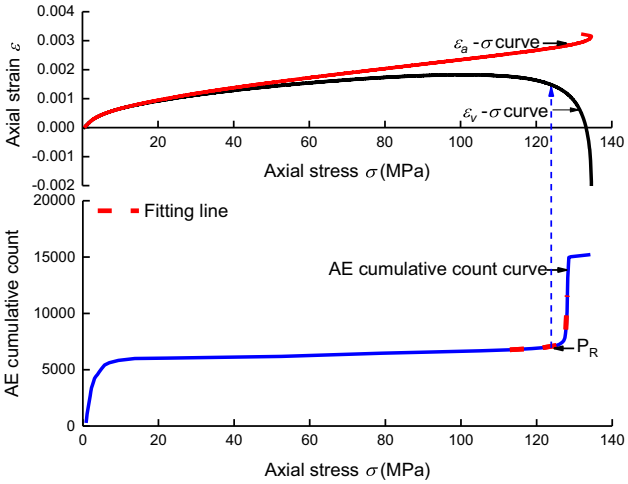

(j) Leiyang white marble 1

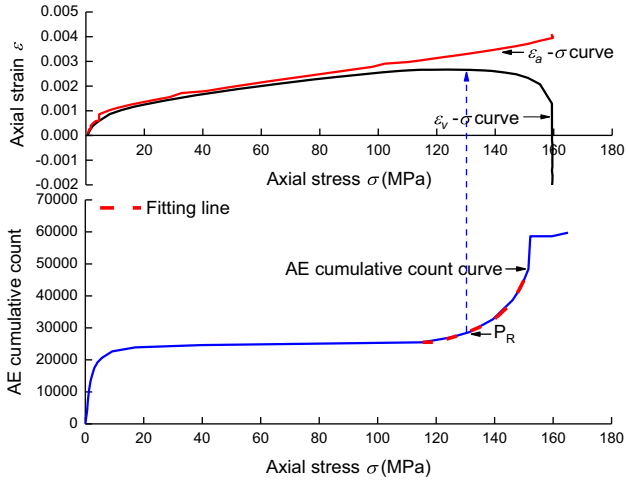

(h) Henan limestone 1

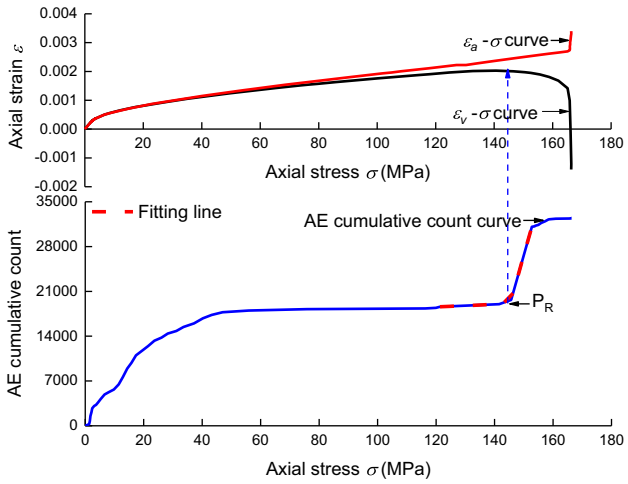

(i) Slate 2

Fig. 10 (continued)

Table 2 R stress and crack damage stress for the different rock materials

Rock type	Number	R stress (MPa)	Damage stress (MPa)	Relative errors (%)
Yueyang granite	1	183.32	181.08	1.24
	2	175.86	179.38	1.96
Fine granite	1	188.21	192.21	2.08
	2	186.34	189.57	1.70
Qingshan granite	1	98.74	115.36	14.41
	2	109.37	118.24	7.50
Red granite	1	102.23	116.83	12.50
	2	108.54	113.51	4.38
Red sandstone	1	91.82	90.48	1.48
	2	89.59	87.58	2.30
Green sandstone	1	76.82	67.13	14.43
	2	66.28	67.48	1.78
Yellow sandstone	1	85.93	80.15	7.21
	2	80.24	76.58	4.78
Henan limestone	1	129.11	130.79	1.28
	2	133.25	134.72	1.09
Slate	1	141.37	139.87	1.07
	2	146.35	142.86	2.44
Leiyang white marble	1	124.02	108.45	14.36
	2	109.51	105.43	3.87

method is the most frequently used method for determining stress thresholds based on AE signals. According to this method, the rock failure process can be divided into different stages by using an auxiliary line, and then the σ_{cd} values of rock materials can be determined (shown in Fig. 12). A specific limitation of this method is that the location of the auxiliary line is greatly influenced by human factors. Additionally, this method cannot quantitatively identify the σ_{cd} values of rock materials.

In this work, the σ_R^{AE} values of the rock materials were identified by using a fitting optimization method based on AE cumulative count curves. The proposed method can quantitatively determine the value of σ_{cd} by using a rigorous mathematical approach. This method is less affected by human factors than previous methods. Additionally, through continuous monitoring of AE signals, the proposed fitting optimization method can be applied to estimate the deformation states of rock. For example, microseismic (MS) monitoring is similar to "in situ" AE testing, a model based on MS monitoring was proposed by relevant scholars to identify the displacement and damage of bedded rock masses (Li et al. 2020). Drawing on the research results of these scholars, the method proposed in this work also be used to assess the damage degree of rock masses. However, further investigation regarding this application is required.

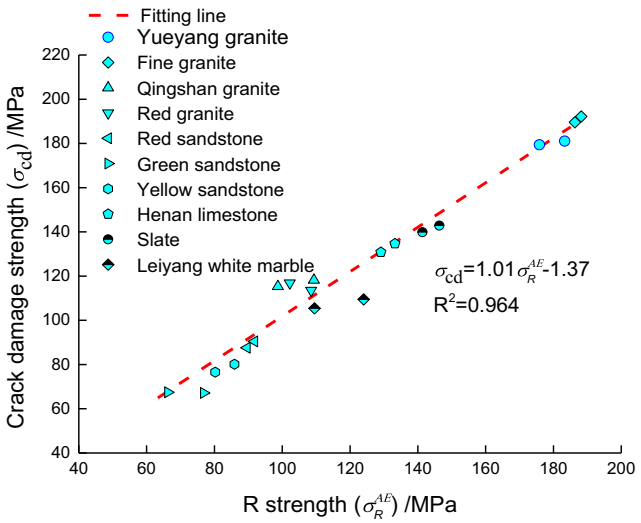

Fig. 11 Fitting relationship between R stress and damage stress for ten rocks

Conclusions

AE signals are transient elastic waves caused by the development of damage (e.g., cracks) in solid materials under loading (Pestman and Munster 1996; Gong et al. 2019). For the

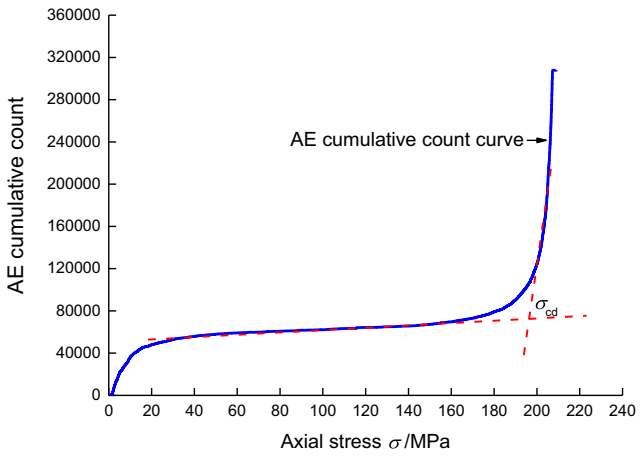

Fig. 12 AE cumulative count method to establish crack stress thresholds

compression process of rock materials, real-time and uninterrupted detection of AE signals can be used to investigate the initiation and development of fractures in rock. Based on the above analysis, the investigation of AE cumulative count was introduced to identify the crack stress thresholds in the rock damage process. Additionally, the relationship between σ_R^{AE} and σ_{cd} was analyzed. The following conclusions were drawn from this study:

(1) In this work, the AE signals of ten rock materials were monitored in real-time during uniaxial compression tests. The relationship between the AE counts and the AE cumulative count curves of different rock materials was studied. The results showed that the AE cumulative count curve can be roughly divided into three stages as the axial stress increases: the slowly increasing stage, the steady stage, and the sharply increasing stage.
(2) The inflection point between the steady stage and the sharply increasing stage was identified as the P_R point. The P_R point of the AE cumulative count curve could be determined based on the fitting optimization method. Moreover, the axial stresses corresponding to the P_R point were defined as σ_R^{AE}.
(3) The values of σ_{cd} for the ten rock materials were obtained using the crack volumetric strain model. Moreover, the relationship between σ_R^{AE} and σ_{cd} was investigated for the ten rock materials. The fitting coefficient of the $\sigma_R^{AE} - \sigma_{cd}$ fitting line was 0.964, which indicates that there is a clear correspondence between σ_R^{AE} and σ_{cd}. Furthermore, σ_R^{AE} can be used to determine the value of σ_{cd} and the starting point of the dilation stage of rock materials.

Funding information This work was supported by the National Natural Science Foundation of China (Grant No. 41877272 and 41472269).

Appendix

Program for the fitting optimization method is as follows:

Program for the fitting optimization method is as follows:

```
%input=xlsread('Workbook of AE cumulative count-axial stress data.xlsx');
x=input(:,1);y=input(:,2); sv=abs(x-max(x)/2); startpoint=find(min(sv)==sv); % x σ /MPa y AE cumulative count
leng=length(input)-startpoint;
per=floor(0.01*leng); % 0.01 scope of data reduction at a time
xrange1=x(startpoint:end); % the original scope of x
yrange1=y(startpoint:end); % the original scope of y
xrange=xrange1;
yrange=yrange1;
p=polyfit(xrange,yrange,4); % fitted by a fourth-degree polynomial
yv=polyval(p,xrange);
R=corrcoef(yrange,yv);R=R(1,2); % initial correlation coefficient
while R <0.996
    frange=1:per;
    brange=(leng-per+1):leng;
    fsum=abs(sum(yrange(frange)-yv(brange)));
    bsum=abs(sum(yrange(brange)-yv(brange)));
    if fsum>bsum
        xrange(frange)=[];
        yrange(frange)=[];
    else
        xrange(brange)=[];
        yrange(brange)=[];
    end
    [p1,S]=polyfit(xrange,yrange,4);
    yv1=polyval(p1,xrange);
    R=corrcoef(yrange,yv1);
    R=R(1,2);
    leng=length(xrange); % update the range of x y
```

References

Cai M, Kaiser PK, Tasaka Y, Maejima T, Morioka H, Minami M (2004) Generalized crack initiation and crack damage stress thresholds of brittle rock masses near underground excavations. Int J Rock Mech Min Sci 41(5):833–847

Cai M, Kaiser PK, Morioka H, Minami M, Maejima T, Tasaka Y, Kurose H (2007a) FLAC/PFC coupled numerical simulation of AE in large-scale underground excavations. Int J Rock Mech Min Sci 44:550–564

Cai M, Morioka H, Kaiser PK, Tasaka Y, Kurose H, Minami M, Maejima T (2007b) Back-analysis of rock mass strength parameters using AE monitoring data. Int J Rock Mech Min Sci 44(4):538–549

Cai M (2010) Practical estimates of tensile strength and Hoek–Brown strength parameter mi of brittle rocks. Rock Mech Rock Eng 43(2):167–184

Chen G, Jiang W, Sun X, Zhao C, Qin C (2019) Quantitative evaluation of rock brittleness based on crack initiation stress and complete stress–strain curves. Bull Eng Geol Environ 78:5919–5936

Diederichs MS, Kaiser PK, Eberhardt E (2004) Damage initiation and propagation in hard rock during tunnelling and the influence of near-face stress rotation. Int J Rock Mech Min Sci 41(5):785–812

Du H, Dai F, Xu Y, Yan Z, Wei M (2020) Mechanical responses and failure mechanism of hydrostatically pressurized rocks under combined compression-shear impacting. Int J Mech Sci 165:105219

Eberhardt E, Stead D, Stimpson B, Cornwall TR (1997) Changes in acoustic event properties with progressive fracture damage. Int J Rock Mech Min Sci 34(3):633

Eberhardt E, Stead D, Stimpson B, Read RS (1998) Identifying crack initiation and propagation thresholds in brittle rock. Can Geotech J 35(2):222–233

Eberhardt E, Stead D, Stimpson B (1999) Quantifying progressive pre-peak brittle fracture damage in rock during uniaxial compression. Int J Rock Mech Min Sci 36:361–380

Gong FQ, Wu C (2019) Identifying the crack compaction strength and damage strength of rock materials using load–unload response ratio theory. Rock Mech Rock Eng:1–12

Gong FQ, Wu C, Luo S, Yan J (2019) Load-unload response ratio characteristics of rock materials and their application in prediction of rockburst proneness. Bull Eng Geol Environ 78:5445–5466

Huang D, Li XQ (2017) Numerical simulation research on characteristic strength of marble based on development of microcrack. Rock Soil Mech 38(1):254–262 (in Chinese)

Koerner RM, Mccabe WM, Lord AE (1981) Overview of acoustic emission monitoring of rock structures. Rock Mech Rock Eng 14(1):27–35

Kong R, Feng XT, Zhang XW, Yang CX (2018) Study on crack initiation and damage stress in sandstone under true triaxial compression. Int J Rock Mech Min Sci 106:117–123

Li A, Liu Y, Dai F, Liu K, Wei M (2020) Continuum analysis of the structurally controlled displacements for largescale underground caverns in bedded rock masses. Tunn Undergr Sp Tech 97:103288

Liu Y, Dai F, Dong L, Xu NW, Feng P (2018) Experimental investigation on the fatigue mechanical properties of intermittently jointed rock models under cyclic uniaxial compression with different loading parameters. Rock Mech Rock Eng 51(1):47–68

Liu QS, Hu YH, Liu B (2009) Progressive damage constitutive models of granite based on experimental results. Rock Soil Mech 30(2):289–296 (in Chinese)

Liu XD, Dai SG, Mu PA (2013) The research and application on light shape detection of car's headlamp. Appl Mech Mater 483:391–396

Martin CD, Chandler NA (1994) The progressive fracture of Lac du Bonnet granite. Int J Rock Mech Min Sci Geomech Abstr 31(6):643–659

Martin CD (1993) The strength of massive Lac du Bonnet granite around underground openings. Ph.D. thesis, Manitoba, Canada: University of Manitoba

Martin CD (1997) Seventeenth Canadian geotechnical colloquium: the effect of cohesion loss and stress path on brittle rock strength. Can Geotech J 34(5):698–725

Mlakar V, Hassani FP, Momayez M (1993) Crack development and acoustic emission in potash rock. Int J Rock Mech Min Sci Geomech Abstr 30(3):305–319

Moradian ZA, Ballivy G, Rivard P, Gravel C, Rousseau B (2010) Evaluating damage during shear tests of rock joints using acoustic emissions. Int J Rock Mech Min Sci 47(4):590–598

Nicksiar M, Martin CD (2012) Evaluation of methods for determining crack initiation in compression tests on low-porosity rocks. Rock Mech Rock Eng 45(4):607–617

Nicksiar M, Martin CD (2013) Crack initiation stress in low porosity crystalline and sedimentary rocks. Eng Geol 154:64–76

Peng J, Yuen WLN, Guang L, Ing TC (2018) Influence of initial micro-crack damage on strength and micro-cracking behavior of an intrusive crystalline rock. Bull Eng Geol Environ 78:2957–2971

Pepe G, Mineo S, Pappalardo G, Cevasco A (2018) Relation between crack initiation-damage stress thresholds and failure strength of intact rock. Bull Eng Geol Environ 77:709–724

Pestman BJ, Munster JGV (1996) An acoustic emission study of damage development and stress-memory effects in sandstone. Int J Rock Mech Min Sci Geomech Abstr 33(6):585–593

Wang B, Zhu J, Peng Y, Huang S, Wu A (2012) Damage strength determination of marble and its parameters evaluation based on damage control test. Chin J Rock Mech Eng 31:3967–3973 (in Chinese)

Wang Y, Li X (2015) Experimental study on cracking damage characteristics of a soil and rock mixture by UPV testing. Bull Eng Geol Environ 74(3):775–788

Wei MD, Dai F, Xu NW, Zhao T, Xia KW (2016) Experimental and numerical study on the fracture process zone and fracture toughness determination for ISRM-suggested semi-circular bend rock specimen. Eng Fract Mech 154:43–56

Wei MD, Dai F, Xu N, Zhao T, Liu Y (2017a) An experimental and theoretical assessment of semi-circular bend specimens with chevron and straight-through notches for mode I fracture toughness testing of rocks. Int J Rock Mech Min Sci 99:28–38

Wei MD, Dai F, Xu NW, Liu Y, Zhao T (2017b) Fracture prediction of rocks under mode I and mode II loading using the generalized maximum tangential strain criterion. Eng Fract Mech 186:21–38

Wen T, Tang HM, Ma JW, Wang YK (2018) Evaluation of methods for determining crack initiation stress under compression. Eng Geol 235:81–97

Yang SQ, Huang YH, Tian WL, Zhu JB (2017) An experimental investigation on strength, deformation and crack evolution behavior of sandstone containing two oval flaws under uniaxial compression. Eng Geol 217:35–34

Zhang JZ, Zhou XP, Zhou LS, Berto F (2019) Progressive failure of brittle rocks with non-isometric flaws: insights from acousto-optic-mechanical (AOM) data. Fatigue Fract Eng Mat Struct 42(8):1787–1802

Zhang XP, Wong LNY (2013) Crack initiation, propagation and coalescence in rock-like material containing two flaws: a numerical study based on bonded-particle model approach. Rock Mech Rock Eng 46(5):1001–1021

Zhou H, Meng FZ, Lu JJ (2014) Discussion on methods for calculating crack initiation strength and crack damage strength for hard rock. Rock Soil Mech 4:913–920 (in Chinese)

Zhou X, Ha Q, Zhang Y, Zhu K (2004) Analysis of deformation localization and the complete stress–strain relation for brittle rock subjected to dynamic compressive loads. Int J Rock Mech Min Sci 41(2):311–319

Zhou XP (2005) Localization of deformation and stress–strain relation for mesoscopic heterogeneous brittle rock materials under unloading. Theor Appl Fract Mech 44(1):27–43

Zhou XP, Zhang YX, Ha QL, Zhu KS (2008) Micromechanical modelling of the complete stress–strain relationship for crack weakened rock subjected to compressive loading. Rock Mech Rock Eng 41(5): 747–769

Zhou XP, Wang YT (2016) Numerical simulation of crack propagation and coalescence in pre-cracked rock-like Brazilian disks using the non-ordinary state-based peridynamics. Int J Rock Mech Min Sci 89:235–249

Zhou XP, Zhang JZ, Qian QH, Niu Y (2019) Experimental investigation of progressive cracking processes in granite under uniaxial loading using digital imaging and AE techniques. J Struct Geol 126:129–145

Zhu ZM, Mohanty B, Xie HP (2007) Numerical investigation of blasting-induced crack initiation and propagation in rocks. Int J Rock Mech Min Sci 44(3):412–424